SAND2016-2028C

Western States Section of the Combustion Institute – Spring 2016 Meeting
Hosted by University of Washington
March 21-22, 2016

Soot formation during high-pressure pyrolysis of n-dodecane sprays

Koji Yasutomi *Scott A. Skeen*

Combustion Research Facility, Sandia National Lab, 7011 East Ave. Livermore, CA 94550

Abstract

Soot formation in pyrolyzing sprays of n-dodecane is visualized and quantified in a high-pressure, high-temperature, constant-volume spray chamber at pressures relevant to modern compression ignition engines. Sprays of n-dodecane are injected at 500 bar from a single-hole, 186-µm orifice diameter, diesel injector belonging to the family of Engine Combustion Network (ECN) Spray D injectors. We quantify the temporal evolution of the total soot mass formed in the pyrolyzing sprays using a high-speed extinction imaging diagnostic. The ambient temperature and pressure of the nearly quiescent flow into which the sprays are injected are varied independently to identify a soot "onset" temperature for n-dodecane pyrolysis and to explore potential pressure dependencies of this limit. Radiation corrected temperatures measured at three axial locations near the radial boundary of the penetrating spray using a fine-wire Type-R thermocouple provide a relation between the bulk temperature measured by a pressure transducer and the core temperature driving soot formation. This relation is used to determine the soot onset temperature. The time-resolved total soot mass is further evaluated to determine pressure dependencies on the rate of soot formation.

INTRODUCTION

Soot emissions from direct-injection diesel engines have been greatly reduced over the last two decades through improvements to fuel injectors, air handling, piston bowl geometries, and the development and deployment of the diesel particulate filter (DPF); however, more stringent emissions requirements are forthcoming that will require engine manufacturers to develop means for further reductions. For spark ignition (SI) engines, the advent of gasoline direct-injection (GDI) strategies has proven effective toward improved fuel economy at the cost of higher soot emissions. In particular, efficiency gains in GDI engines can be attributed to 1) reduced pumping losses, 2) leaner global fuel/air equivalence ratios, 3) charge cooling via the fuel spray's latent heat of vaporization, 4) reduced heat loss to the cylinder walls as high-temperature combustion occurs in the region of the fuel spray, and 5) an ability to achieve higher compression ratios without knock. Relative to port fuel injected (PFI) SI engines, however, soot emissions from GDI engines can be elevated because the direct-injection results in an inhomogeneous fuel and air mixture and pool-type combustion can occur on wetted cylinder surfaces during cold engine start-up [1,2,3,4]. If combustion generated soot cannot be sufficiently reduced in-cylinder, GDI engines may require the addition of a gasoline particulate filter (GPF). Similar to the DPF for diesel engines, the after treatment equipment will result in higher vehicle cost and decreased fuel economy [5]. Moreover, there is impetus to minimize GDI in-cylinder soot to reduce radiative heat loss to further improve efficiency gains [6].

Considerable effort and financial resources have been expended toward the development of predictive models that will enable the efficient and cost-effective design of advanced engines capable of meeting future fuel economy and emissions mandates. Detailed chemical mechanisms describing the decomposition and oxidation of hydrocarbon fuel components found in commercial gasoline and diesel can contain thousands of species and tens-of-thousands of reactions. Implementing such large mechanisms in CFD codes can be computationally overwhelming, therefore the mechanisms are typically reduced by an order of magnitude or more before CFD calculations are performed. In the engines and spray combustion modeling communities, these reduced mechanisms are commonly supplemented with simplified two-step soot formation mechanisms [7]. While more complex soot formation mechanisms have been developed, there has been no conclusive determination of the physicochemical process by which gas phase molecules nucleate into the first soot particles, i.e., soot inception. The present work explores the potential for furthering our understanding of soot inception under engine relevant conditions by quantifying soot formed in pyrolyzing sprays of n-dodecane in a constant volume, high-pressure spray vessel. The specific objectives of this work are to quantify the reproducibility of soot formation from pyrolysis at ambient temperatures above those normally considered during combusting spray experiments, identify a soot onset temperature for n-dodecane for comparison with the onset temperature identified along the centerline of atmospheric co-flow diffusion flames, and distinguish mixing effects from kinetic effects as the ambient pressure (and therefore density) is increased.

Gomez et al. [8] and Saito et al. [9] measured average soot "onset" temperatures of 1350 K and 1365 K, respectively, along the centerline of co-flow diffusion flames burning a variety of hydrocarbon fuels. The onset temperature was defined by the radiation corrected temperature at the highest axial location prior to soot deposition onto the thermocouple. Of the 12 flames studied in Gomez et al. [8], all were established at the smoke height condition with the exception of one of the

five butene flames. Saito et al. [9] indicated that small diffusion flames were selected for their study since such flames remain in the early stage of soot formation. For all cases in Gomez et al. [8], the soot onset location was observed at a height in the flame between 25% and 40% of the luminous flame height and Saito et al. [9] reported that the first soot deposits onto their probe occurred between 2 mm and 4 mm below the first visible appearance of yellow emission. We note that early soot processes along the centerline of a co-flow diffusion low in the flame are more representative of a pyrolysis pathway since these regions are oxygen deficient. As such, the temperatures measured by Gomez et al. [8] and Saito et al. [9] provide an interesting reference for the present study of pyrolyzing sprays. It should be noted that other experimental studies have identified an "inception" temperature near 1600 K. Whereas the onset temperature described above has been measured in a region where soot formation is not greatly influenced by oxidation processes, studies referencing the inception temperature have generally been conducted under conditions where competition between soot formation and oxidation occurs [10,11,12].

Frenklach et al. [13,14] investigated soot formation under pyrolyzing conditions for several fuels diluted with argon in a shock tube. Using laser extinction, they measured the time evolution of soot conversion as a function of the temperature and pressure behind the reflected shock wave. The time-dependent soot yield showed an S-shaped character representative of an autocatalytic process. Temperature dependencies were characterized by a "bell-shaped" distribution—initially increasing as the temperature behind the reflected shock increased but then decreasing after the temperature reached 1800 K - 2000 K. The peak in the distribution was dependent upon the observation time and wavelength of incident laser light used for the extinction measurements. Small soot yields were observed below 1600 K in toluene studies at a pressure of 2.5 bar with an extrapolated "onset" temperature near 1500 K. Increasing pressure from sub-atmospheric to approximately 7 bar resulted in a slight increase in soot yield, with the effect more pronounced in the lower pressure range. In general, the peak soot yields shift to higher temperatures for lower pressure conditions. For the aromatic (toluene) fuel studied in Ref. [13], it was suggested that the observed temporal behavior and pressure dependencies provides a strong indication that soot formation for aromatics is dominated by kinetics rather than equilibrium processes.

Gülder et al. [15] found that the maximum soot yield in laminar co-flow diffusion flames of methane and ethane increases with pressure, but approaches an asymptote at pressures greater than 20-30 bar. Propane flames were also studied, but the pressure was limited to around 7 bar and asymptotic behavior was not yet achieved. The increased soot yield at higher pressures was attributed to steeper radial temperature gradients leading to more rapid thermal diffusion toward the flame centerline and therefore accelerated soot nucleation and growth. To our knowledge, the asymptotic behavior was not explained. In a flame environment, this asymptotic behavior might be expected since soot formation must compete with oxidation. Specifically, if increased pressures enhance soot oxidation reactions to a greater degree than soot formation reactions, an asymptote (and eventually a decreasing trend) may be observed.

To explore the effect of temperature and pressure on soot formation rates and the possibility that a pressure invariant soot "onset" temperature near 1350 K exists, we investigate soot formation in pyrolyzing sprays of n-dodecane in a constant volume, high-pressure, high-temperature chamber. Several ambient temperatures are explored at three ambient pressures (38.2 bar, 76.4 bar, and 114.6 bar). Radiation corrected thermocouple temperature measurements were performed at three axial

locations within a few millimeters of the penetrating vapor boundary to assess temperature fluctuations and to provide a correlation between the "core" temperature observed by the spray and the "bulk" temperature derived from the measured vessel pressure. The time evolution of the total soot mass was quantified using a high-speed, diffused back-illumination extinction imaging (DBIEI) diagnostic. To distinguish the potential impact of enhanced mixing at the higher ambient pressure (and therefore density) conditions from enhanced kinetics due to pressure, we simulated the penetration and mixing of the spray using a one-dimensional jet model.

EXPERIMENTAL SETUP

Combustion Vessel and Injection System

Sprays of n-dodecane were injected into an optically accessible constant-volume combustion vessel. The vessel is nearly cubical with an internal volume of approximately one liter and achieves pressures and temperatures relevant to modern CI engines via the combustion of a premixed charge. Following this "pre-burn" event, a cool-down period ensues resulting in a time-dependent range of thermodynamic conditions into which the fuel spray can be injected. A detailed description of the vessel and its operation can be found in Siebers [16]. Figure 1 provides visual information about the layout of the vessel and its optical access.

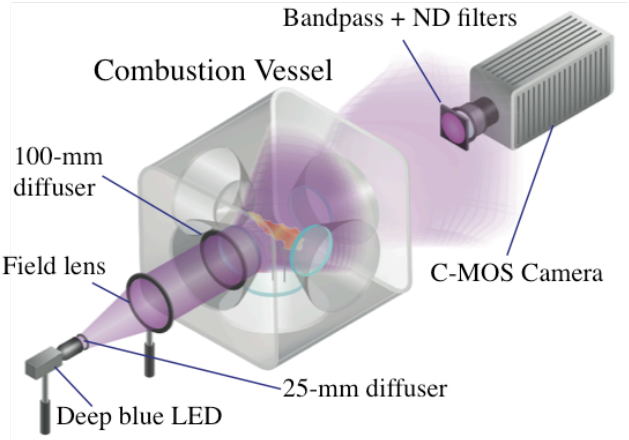

Figure 1. Schematic diagram of the high combustion vessel and optical arrangement.

Fuel was injected using a common-rail diesel fuel injector equipped with a single 186-μm diameter orifice (#209134) belonging to the family of Spray D injectors from the Engine Combustion Network (ECN) [17]. The Spray D nozzle features a conically-shaped orifice with a *k-factor* of 1.5. Following the ECN specifications, the injector was housed in a water-cooled mount maintaining the fuel temperature at the nozzle at 90 °C. For the present experiments, the injection pressure was fixed at 500 bar and a 290 μs electronic "ramp" signal was supplied to the injector to limit the spray penetration and the mass of fuel injected. The 290 μs electronic ramp signal supplied to the injector was controlled by a Genotec injector driver with a ramp current of 20 A, and a ramp hysteresis of 1 A.

All experiments were conducted in an inert environment (i.e., no molecular oxygen) to focus on soot formed by pyrolysis. A range of ambient temperatures over three ambient pressures were considered as detailed in Table 1.

Table 1. Experimental conditions.

T_a [K]: ambient temperature	1400	1450	1500	1550	1600	1650	1700
P_a[bar]: ambient pressure		38.2		76.4	114.6		
O_2 concentration [vol.%]				0			

Diffused Back-Illumination Extinction Imaging (DBIEI)

Soot particles formed following pyrolytic decomposition of n-dodecane are measured using a high-speed imaging extinction method. The main components of this diagnostic consist of a high-output, ultra-fast, deep blue (406-nm, 17-nm FWHM) light emitting diode (LED) equipped with a collimator, two engineered diffusers, a field lens, and a high-speed camera. The first engineered diffuser is mounted at the exit of the LED collimator and has a 25-mm diameter and a circular 50-degree distribution. The light passing through this first diffuser is collected by the 150-mm diameter, 150-mm focal length field lens. The field lens directs the nearly collimated light to the second diffuser, which has a 100-mm diameter and a circular 15-degree distribution. The high speed camera is operated at 50,000 frames per second and is equipped with a 50-mm f/1.2 Nikkor lens, a 500D close-up lens, a 400-nm (25-nm FWHM) bandpass filter, and an OD 1.5 neutral density filter. The light source setup described above directs the diffused illumination toward the spray plane with a quasi-Lambertian distribution, resulting in minimal light extinction induced by beam steering through the chamber and spray flame because of density (temperature) gradients.

The LED is pulsed in every other camera frame to permit the removal of sensor background signal and broadband emission from hot soot particles at each time step. The extinction images are converted into 2-D maps of optical thickness (KL) using the Beer-Lambert law, $I/I_0 = \exp(-KL)$, where I and I_0 are the transmitted and incident illumination intensities, respectively, K is the dimensional extinction coefficient of soot, and L is the path length through the soot cloud. Example KL images showing the time evolution of soot optical thickness in a pyrolyzing spray at ambient conditions corresponding to 38.2 bar and 1550 K condition are provided in the left column of Figure 2. These images represent an ensemble average of five repeated runs at the same target condition. The KL maps can be related to the total soot mass in the spray at each time step after determining an appropriate value for the non-dimensional extinction coefficient as discussed by Manin et al. [18]. In addition to carefully optimized illumination and imaging setups, the images have been corrected during post-processing to account for negative image lag associated with the high-speed camera and variation in illumination intensity. More information concerning the implementation and performance of the DBIEI diagnostic can be found in Ref. [19].

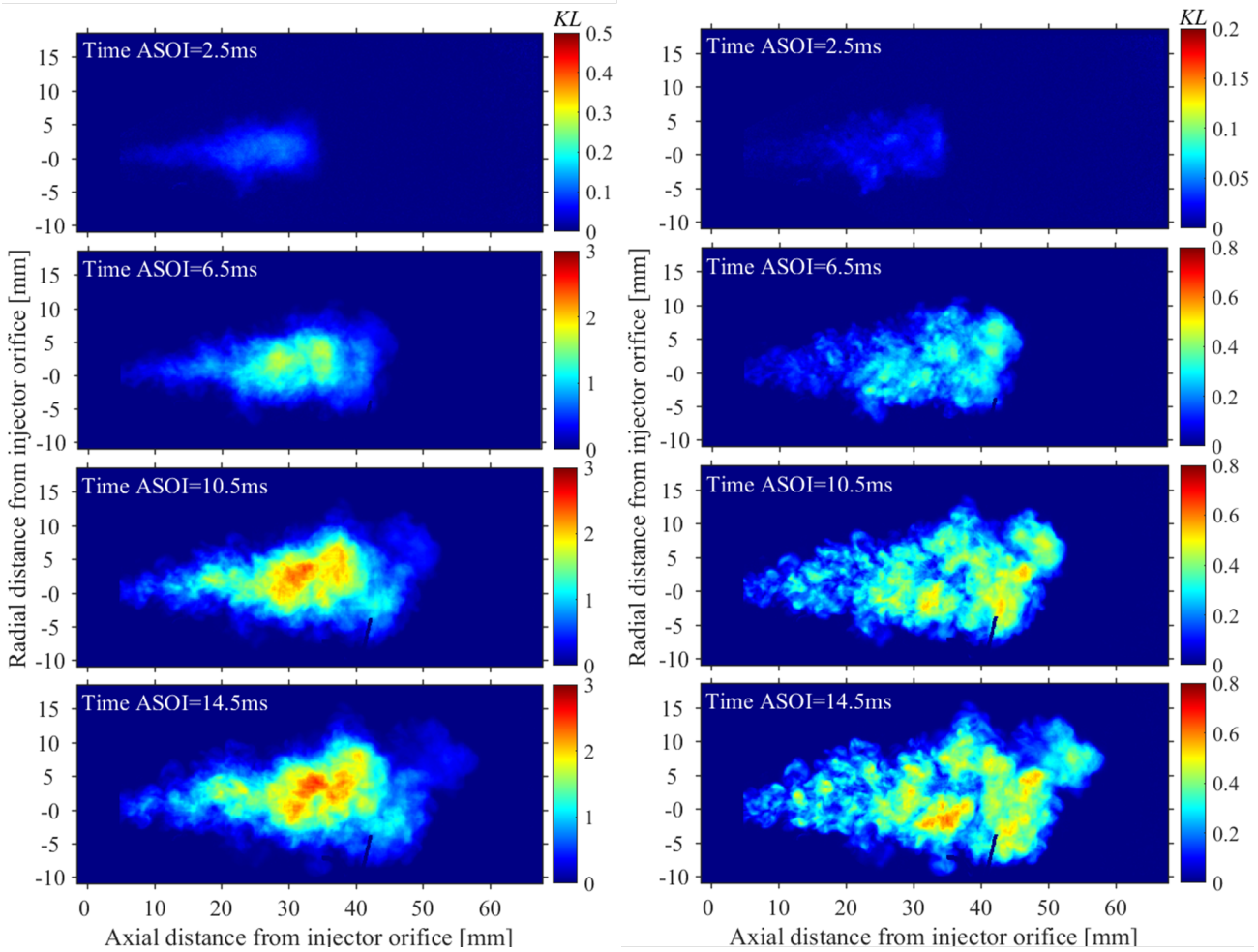

Figure 2. (Left panels) Ensemble averaged *KL* of five repeated experiments at four different timings after the start of injection (ASOI). (Right panels) Standard error (SE) of *KL* for the five repeated experiments at four different times ASOI. The ambient temperature and pressure were 1550 K and 38.2 bar, respectively.

Gas Temperature

The gas temperatures at three axial locations along the spray axis just below the vapor boundary were measured during each pre-burn and injection event using fine-wire (50-µm diameter) platinum/platinum-rhodium (type-R) thermocouples. These temperature measurements were used to provide insight into the variability of temperatures in and around the entrainment zones and to provide a core-to-bulk relationship as is commonly adopted in pre-burn vessels to determine temperature from pressure measurements. The thermocouples were mounted on the bottom vessel window with the beads located at the positions listed in Table 2 and radiation corrections were performed. The dimensions of the thermocouples were chosen to minimize several sources of error, while also surviving repeated premixed burn and cool down periods in the combustion vessel. Small diameter wires are needed to minimize errors caused by thermal inertia, radiation, and conduction [20]. Some discussion on the repeatability of temperatures is provided in the next section.

Table 2. Thermocouples setting position in the vessel.

	Tc_1	Tc_2	Tc_3
X [mm]: Spray axis direction from the tip	11.4	39.3	82.3
Y [mm]: Spray radius direction from the tip	4.7	6	11.1

Reproducibility of pre-burn vessel data during spray pyrolysis

Ambient temperatures and pressures within the pre-burn type constant volume spray vessel are easily manipulated relative to a shock tube configuration. Nevertheless, non-uniformities in the temperature distribution are expected due to turbulence remaining from the pre-burn flame propagation and buoyancy. The ratios of the mean measured temperatures to the bulk temperature, computed from the measured vessel pressure, are presented in Figure 3 for the 38.2 bar and 1550 K condition.

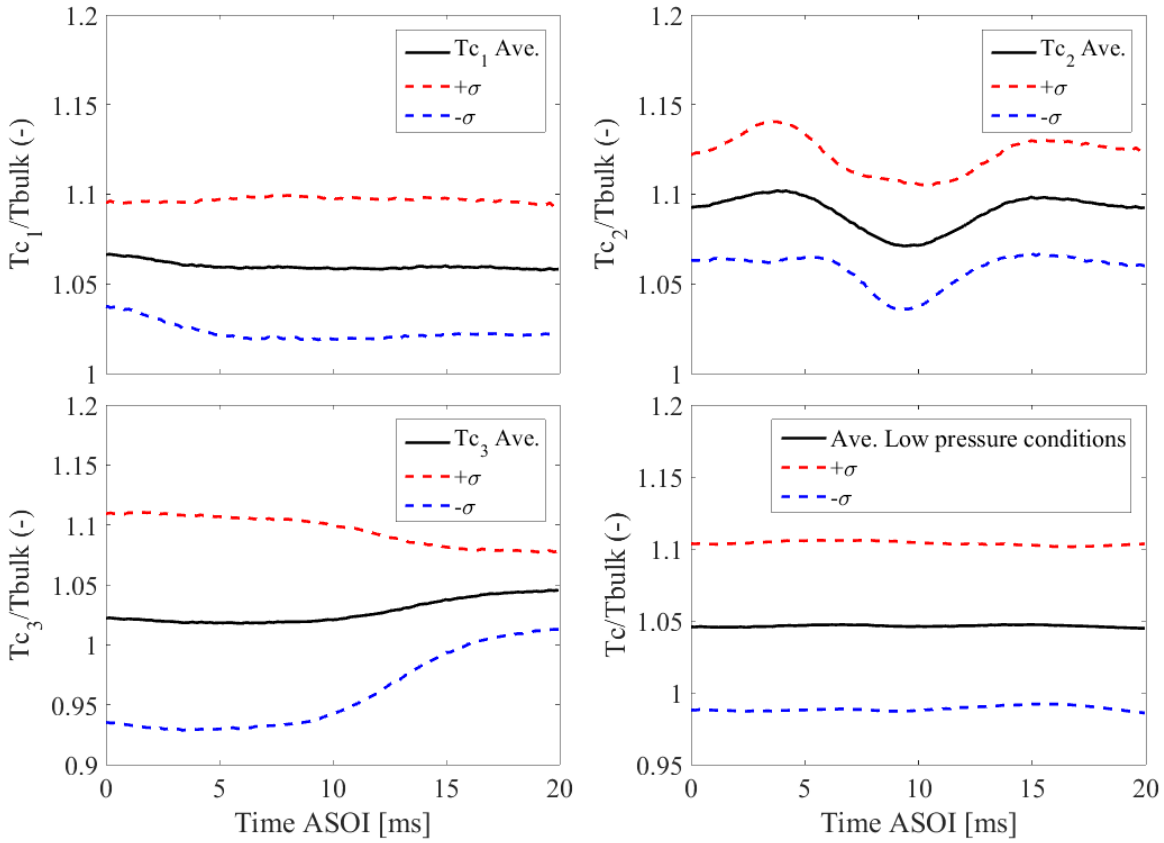

Figure 3. The top two panels and bottom left panel show the ensemble averaged thermocouple temperatures relative to the bulk temperature (computed from the measured pressure) for 20 ms after the start of injection for the 1550 K, 38.2 bar condition. The bottom left panel shows the ensemble average of all three thermocouples for all ambient conditions studied at the 38.2 bar condition. The dashed lines represent the standard deviation.

As was the case for Fig. 2, the data in Fig. 3 represent an ensemble average of five events. Due to heat loss through the vessel walls, thermocouple temperatures measured near the center or "core" of the vessel are expected to be higher than the bulk temperature determined from the measured pressure. Temperature data out to 20 ms ASOI are included to demonstrate that the core-to-bulk relationship is relatively constant during the injection event and for a significant time thereafter with

a standard deviation of just a few percent. Though not shown here, the core temperature drops a maximum of 1.4% during this 20 ms interval for the 1700 K ambient condition. For the 1400 K condition, the temperature drops less than 1%. During post-processing and data analysis, it was determined that local temperature fluctuations captured by the thermocouples could lead to poor correlation between the observed soot characteristics and the targeted boundary conditions. Better correlation was observed by considering the core temperature as determined from the bulk-to-core relationship on a case-by-case basis.

In addition to temperature stratification in the ambient as a source of shot-to-shot variation, turbulent fluctuations in high-pressure sprays are a dominant source of spatial variation of the measured *KL* maps shown previously in Fig. 2. Returning to the right column of panels in Fig. 2, we present the standard error (SE) of the five repeated events at four different times ASOI. As we will demonstrate in the next section, the large variation among these repeated experiments is mainly attributable to the stochastic nature of the turbulent spray leading to a random spatial distribution of soot. By considering the total soot mass, which is an integrated quantity throughout the entire volume of interest, the variability among repeated experiments is greatly reduced.

RESULTS AND DISUCUSSION

Ambient temperature effects

The total soot mass as a function of time ASOI at an ambient pressure of 38.2 bar for seven different ambient temperatures is presented in Figure 4. The left panel includes the ensemble-averaged total soot mass as a function of time for three or more repeated injections having the same target ambient conditions (38.2 bar, 1400-1700 K) and the same quantity of fuel injected. In the right figure panel we provide the time-resolved standard error for each case. Whereas the standard error of the *KL* images reached values as high as 26% of the ensemble-average, the SE of the total soot mass remains below 10%. For the other ambient conditions of this study, similar consistency was observed for repeated experiments.

As expected, the peak rate of soot mass formation increases at higher ambient temperatures as observed by Frenklach et al. [13,14] in a shock tube over a range of reflected shock temperatures from 1495 K to 1729 K; however, because 1700 K represents the peak ambient temperature of the present study, we are not able to confirm their observation that the soot yield diminishes above some characteristic temperature. Nevertheless, for ambient temperatures of 1500 K and above the total soot mass reaches nearly the same value suggesting that our maximum ambient temperature (1700 K) is approaching the characteristic temperature for diminishing soot yield or soot yield is limited by a factor other than temperature. This will be considered in future work. Finally, the S-shaped character of the time-resolved total soot mass is consistent with the shock-tube experiments of Frenklach et al. [13,14] and further establishes the soot formation process as autocatalytic at pressures exceeding those of previous shock tube studies.

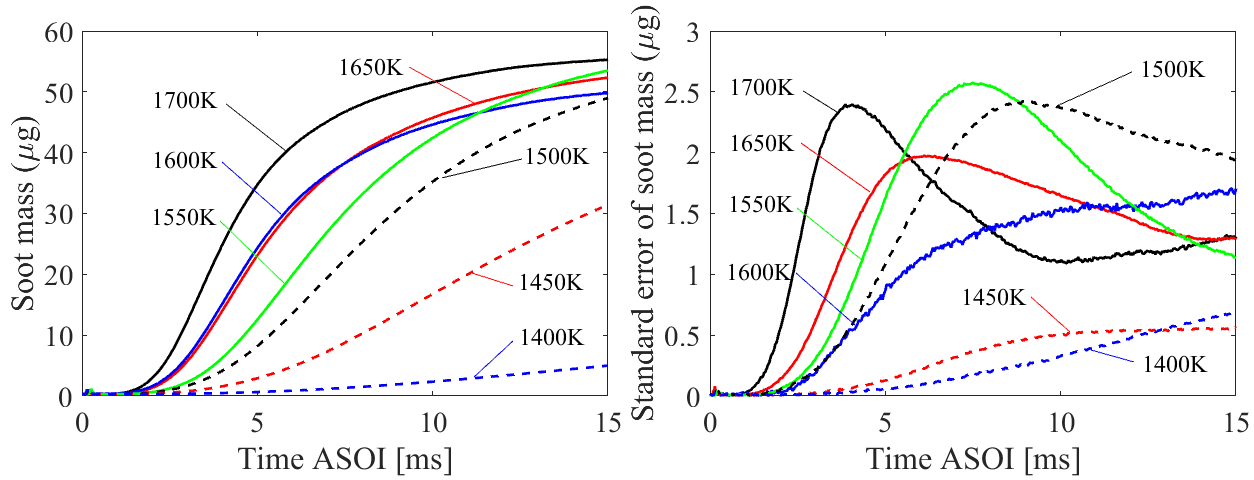

Figure 4. (Left panel) Total soot mass as a function of time ASOI for seven different ambient temperature conditions at an ambient pressure of 38.2 bar. The data have been ensemble averaged over three or more repeated events with the same target conditions. (Right panel) Time evolution of the standard error of the total soot mass.

Ambient pressure effects

To consider potential effects of pressure on the rate of soot formation and establish a characteristic soot onset temperature for pyrolyzing sprays, we varied the ambient temperature at three different fixed ambient pressure conditions. Whereas shock tube experiments involve a well-mixed charge of reactants heated by the passing shock wave, the vaporizing spray is heated during mixing that occurs as ambient gases are entrained [21,22]. As ambient pressure is increased at constant temperature, the increased density results in more rapid entrainment. The higher entrainment rates at higher ambient density mean that the fuel vapor mixes faster with the hot ambient gases and therefore may reach conditions amenable to soot formation earlier than sprays injected into a lower density ambient. For this reason, it is difficult to decouple the potential effect of pressure on the kinetics of soot formation from the effect of mixing in a pyrolyzing spray. To give an impression of the potential impact of enhanced mixing at higher ambient densities on the rate of soot formation in these pyrolyzing sprays, we employed the model of Musculus and Kattke [22]. The model was used to provide an indication of the expected rate of change in mixture fraction. As an input, the model requires a rate-of-injection (ROI) profile in addition to the ambient density, temperature, spreading angle, and injector orifice hydraulic coefficients. Unfortunately, the injection duration increased as the ambient pressure in the chamber increased and the ROI could not be measured with hardware available at the time of this work. The ROI profile and associated mass of fuel injected at the different ambient pressures was therefore estimated iteratively by comparing the experimental penetration with modeled results assuming a constant spreading angle and generating an ROI using the CMT "virtual injector model" [23]. To give an impression of the relative rates of mixing for the three different ambient pressure conditions, in the left panel of Figure 5 we plot the ratio of the cross-sectionally averaged mixture fraction ($\tilde{Z}$) for the 8.26 kg/m^3 and 16.52 kg/m^3 cases relative to the 24.77 kg/m^3 case. Two specific points in the axial distribution at each time step were selected for comparison, namely, the point at which the minimum $\tilde{Z}$ was observed and the point 1 mm upstream of the penetrating head. Initially, the ratios are greater than unity because the higher density condition mixes more rapidly while liquid is being injected. Note however, that increasing the ambient density by a factor of three led to only a 50% (or less) decrease in mixture fraction at these early times. After approximately 100 μs, the

ratios for both lower density conditions pass below unity indicating that the lower density conditions quickly become more mixed than the highest density case. This can be attributed to the shorter injection durations of the lower density cases, which lead to an earlier entrainment wave. At 400 µs ASOI, the ratio for the lowest density case corresponding to the location of minimum $\tilde{Z}$ rises above unity once again as mixing in the highest ambient density case is enhanced by the entrainment wave following the end of this longer injection. Nevertheless, the ratio of $\tilde{Z}$ in the head of the lowest density case remains below unity. For the mid-density case, the ratios at both locations remain below unity indicating that this case remains more mixed than the high-density case throughout the duration of the experiment.

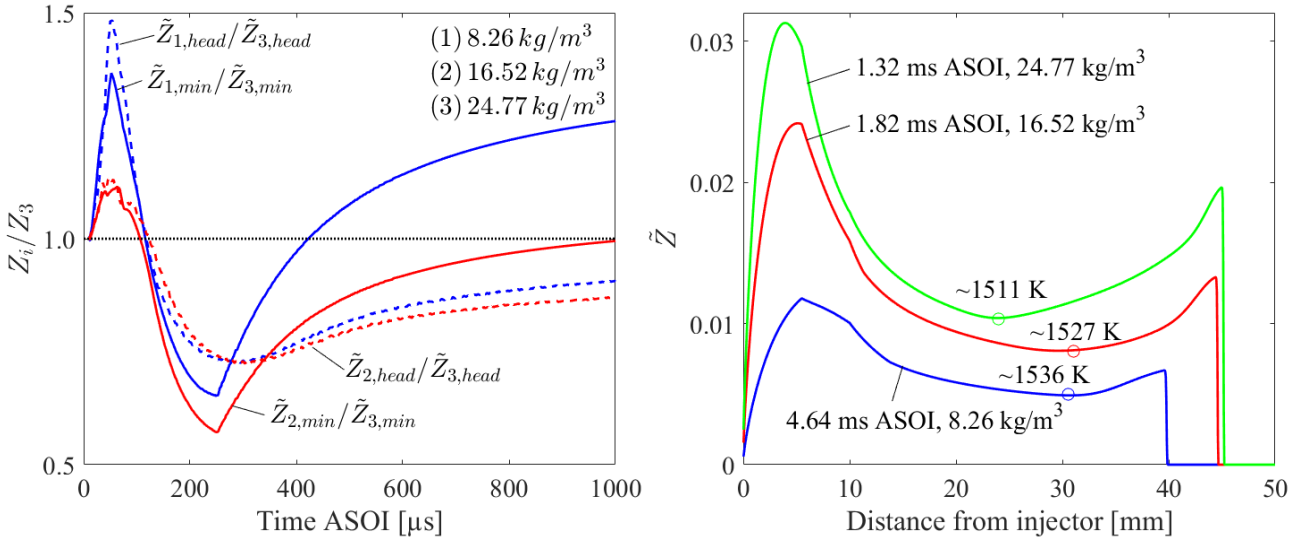

Figure 5. Simulated mixture fraction profiles generated using the one-dimensional model of Musculus and Kattke [22]. (Left panel) Modeled time sequence of the ratio of the cross-sectionally averaged mixture fraction at the minimum point and 1 mm upstream of the head for the low- and mid-density condition relative to the high-density condition. (Right panel) Modeled axial profiles of the cross-sectionally averaged mixture fraction for the three density conditions at times corresponding to the observation of 10 µg of total soot in the experiments at 1550 K.

The right panel of Fig. 5 displays the axial profiles of the cross-sectionally averaged mixture fraction at times corresponding to measured total soot mass of 10 µg for the 1550 K ambient conditions. The highest density (and therefore pressure) condition forms 10 µg of soot slightly earlier than the mid-density condition. Considering that the model showed that the mid-density condition is better mixed for a longer time period preceding the formation of this soot quantity, there is evidence that the increased pressure may lead to faster soot formation at pressures well beyond the asymptotic behavior observed by Gülder et al. [15]. Nevertheless, the result is inconclusive until we can determine if there is some effect related to the larger quantity of fuel injected at the higher density. The data in the right panel also show that the low density condition requires significantly more time to form 10 µg of soot and does so mixture fractions well below the mid- and high-density cases. Under the assumption of adiabatic mixing, both the mid- and low-density conditions would be at only moderately higher temperatures at these times as annotated in the figure. At mixture fractions of 0.01 and below, local temperatures have reached values greater than 95% of the ambient temperature.

In Figure 6, the maximum rate of soot mass formation is plotted against temperature for injections into an ambient at pressures of 38.2 bar, 76.4 bar, and 114.6 bar. The increasing slope in the trend

lines with increasing pressure is consistent with enhanced soot formation kinetics at higher ambient pressures; however, as noted previously further work is needed to completely quantify the effects of enhanced mixing and the mass of fuel injected. At the 1550 K temperature condition, the increased rate of soot formation at the highest pressure condition relative to the lowest pressure case far exceeds the conservative enhancement of a factor of three due to more rapid mixing at higher ambient density. Of particular interest and importance, we observe that the linear extrapolation of these data converge toward a formation rate of zero at temperatures between 1350 K and 1400 K. This finding is consistent with the "onset" temperature measured in atmospheric pressure co-flow flames by Gomez et al. [8] and Saito et al. [9] and further indicates that the onset temperature is pressure invariant for the conditions of this study. Future work will involve investigating the effect of fuel injection duration on the rate of soot mass formation and investigating the onset temperature for a variety of fuels.

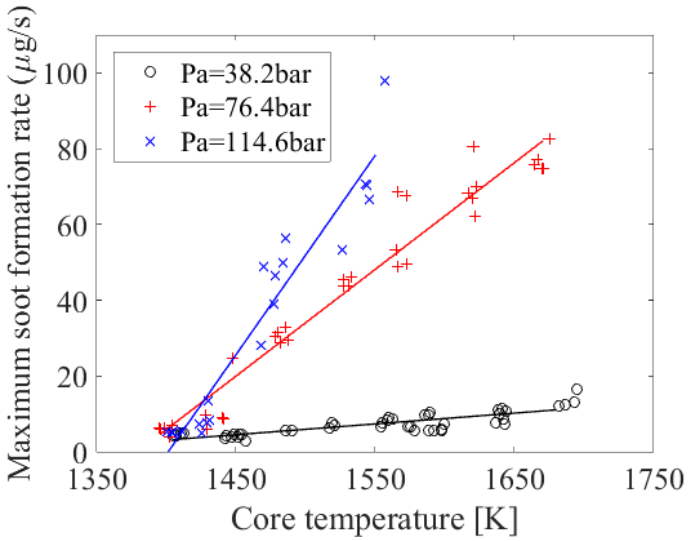

Figure 6. Maximum rate of soot formation as a function of ambient "core" temperature for three different ambient density (pressure) conditions.

SUMMARY AND CONCLUSIONS

Soot formation in pyrolyzing sprays of n-dodecane has been investigated using a constant volume pre-burn vessel. The temporal evolution of the total soot mass was measured by diffused back illumination extinction imaging (DBIEI). Radiation corrected thermocouple measurements provided a core-to-bulk temperature relationship to be used for ambient conditions beyond those explored previously in this experimental apparatus. As expected, the rate of soot formation increased with increasing ambient temperature at constant pressure. Consistent with previous shock tube studies, the soot yield was characterized by an S-type curve as a function of pressure indicative of an autocatalytic process. A critical temperature was observed, above which the ultimate conversion of fuel carbon to soot does not increase with increasing ambient temperature. Future work will pursue higher ambient temperatures to explore diminishing soot yield at temperatures exceeding 1700 K as observed in shock tubes. The effect of pressure on the rate of soot formation was also explored. We used a one-dimensional model for spray penetration and mixing to estimate the potential effect of enhanced mixing at the higher ambient pressure (densities). Inconsistent injector behavior at the

various ambient pressures resulted in smaller amounts of fuel being injected at the lower ambient pressure conditions. The shorter injection durations at the lower density conditions resulted in enhanced mixing due to an earlier arrival of the entrainment wave. The mid-density condition remained more mixed throughout the duration of the event relative to the high-density condition. The higher rate of soot formation observed for the high-density condition is therefore not attributed to enhanced mixing. Further work is necessary to quantify the effect of the greater mass of fuel injected on the maximum rate of soot formation before concluding that pressure is the dominant parameter enhancing soot kinetics. Linear fits through data representing the peak rate of soot formation as a function of temperature for the three different pressure studies appeared to pass through zero at an ambient temperature consistent with the soot "onset" temperature observed previously in atmospheric pressure co-flow diffusion flames.

Acknowledgements

Chris Carlen and Dave Cicone provided technical support for this work. The experiments were conducted at the Combustion Research Facility, Sandia National Laboratories, Livermore, CA. Support for this work was provided by Sandia National Laboratories under the Laboratory-Directed Research and Development (LDRD) program. Sandia is a multi-program laboratory operated by Sandia Corporation, a Lockheed Martin Company, for the United States Department of Energy's National Nuclear Security Administration under contract DE-AC04-94AL85000.

References

[1] Y. Kobayashi and M. Arai, *SAE Int. J. Engines*, vol. 9, no. 1, 2016.

[2] CA. Schuetz and M. Frenklach, *Proc Combust Inst*, vol. 29, no. 2, pp. 2037-2314, 2002.

[3] CL. Myung, H. Lee, K. Choi, YJ. Lee, and S. Park, *Int. J. Automot. Technol.*, vol. 10, no. 5, pp. 537-544, 2009.

[4] S. Zhang and W. McMahon, Sacramento, California, USA, 30 November–2 December 2010.

[5] K. Lee. (2013, May) DOE Annual Merit Review. http://energy.gov/sites/prod/files/2014/03/f13/ace024_lee_2013_o.pdf

[6] S. Skeen, J. Manin, L. Pickett, K. Dalen, and A. Ivarsson, *SAE Technical Paper*, 2014, 2014-01-1252.

[7] H. Hiroyasu and T. Kadota, *SAE paper*, 1976, 760129.

[8] A Gomez, M. G. Littman, and I. Glassman, *Combust Flame*, vol. 70, no. 2, pp. 225-241, 1987.

[9] K. Saito, A. S. Gordon, F. A. Williams, and W. F. Stickle, *Combust. Sci. Tech.*, vol. 80, no. 1-3, pp. 103-109, 1991.

[10] B. M. Kumfer, S. A. Skeen, R. Chen, and R. L. Axelbaum, *Combust Flame*, vol. 147, no. 3, pp. 233-242, 2006.

[11] B. M. Kumfer, S. A. Skeen, and R. L. Axelbaum, *Combust Flame*, vol. 154, no. 3, pp. 546-556, 2008.

[12] I. Glassman, O. Nishida, and G. Sidebotham, *H Bockhorn (Ed.), Soot Formation in Combustion*. Berlin: Springer-Verlag, 1994, P.316.

[13] M, Frenklach, S. Taki, and R. A. Matula, *Combust Flame*, vol. 49, no. 1-3, pp. 275-282, 1983.

[14] M, Frenklach, S. Taki, M. B. Durgaprasad, and R. A. Matula, *Combust Flame*, vol. 54, no. 1-3, pp. 81-101, 1983.

[15] Ö.L. Gülder et al., *Combust Flame*, vol. 158, no. 10, pp. 2037-2044, 2011.

[16] D. Siebers, *SAE Technical Paper 98080*, 1998.

[17] Engine Combustion Network. http://www.sandia.gov/ecn

[18] J. Manin, S. Skeen, L. Pickett, E. Kurtz, and J. E. Anderson, *SAE Int. J. Fuels Lubr*, vol. 7, no. 3, pp. 704-717, 2014.

[19] J. Manin, L. Pickett, and S. Skeen, *SAE Int. J. Engines*, vol. 6, no. 4, 2013, 2013-01-2548.

[20] L. Pickett et al., *SAE Technical Paper*, 2010, 2010-01-2106.

[21] S. Moon, K. Nishida, Y. Matsumoto, and J. Lee, *Atomization and Sprays*, vol. 19, no. 11, pp. 1013-1029, 2009.
[22] M. Musculus and K. Katke, *SAE Int. J. Engines*, vol. 2, no. 1, 2009, 2009-01-1355.
[23] CMT motores térmicos - Virtual injector model. http://www.cmt.upv.es/ECN03.aspx